Smart Mater. Struct. **20** (2011) 055024 (9pp) doi:10.1088/0964-1726/20/5/055024

The actuation characterization of cantilevered unimorph beams with single crystal piezoelectric materials

Onur Bilgen[1], **M Amin Karami**[2], **Daniel J Inman**[2] **and Michael I Friswell**[1]

[1] College of Engineering, Swansea University, Singleton Park, Swansea SA2 8PP, UK
[2] Center for Intelligent Material Systems and Structures, Virginia Tech, Blacksburg, VA 24061, USA

E-mail: o.bilgen@swansea.ac.uk

Received 30 December 2010, in final form 1 April 2011
Published 27 April 2011
Online at stacks.iop.org/SMS/20/055024

Abstract

An experimental and theoretical electromechanical characterization of beam-like, uniform cross-section, unimorph structures employing single crystal piezoelectrics is presented. The purpose of the research is to understand and compare the actuation capabilities of several piezoelectric materials and substrate configurations so that optimal design choices can be employed in lightweight, low power aerodynamic applications. Monolithic devices made from three kinds of piezoelectrics—single crystal PMN–PZT (lead magnesium niobate–lead zirconate titanate) and the polycrystalline PZT-5A and PZT-5H types—are compared in a unimorph cantilevered beam configuration. A total of 24 unimorph specimens are fabricated and the validity of existing models is examined through experimentation. The tip velocity response to harmonic voltage excitation is measured and compared to the analytical prediction with the perfect bonding assumption. Summarizing, it was confirmed that the substrate-to-piezoelectric thickness ratio and substrate modulus are the important design parameters in determining the measured output of the unimorphs and the accuracy of the model prediction. The single crystal piezoelectrics demonstrated actuation authority two to four times higher (measured in terms of peak displacement per applied voltage) when compared to the polycrystalline piezoceramics for the same substrate material and geometry choice. In contrast to the higher actuation output, practical implementation issues are noted for the single crystal devices. The lack of grain boundaries (as in the polycrystalline material) makes the single crystals very 'brittle' and susceptible to stress concentrations. Another important limitation is the low transition temperature, which limits the use of conventional solder materials in creating electrical connections.

(Some figures in this article are in colour only in the electronic version)

1. Introduction

The field of smart materials has advanced rapidly in the last two decades due to an increasing awareness of material capabilities, the development of new materials and transducer designs, and increasingly stringent design and control specifications in aerospace, aeronautic, industrial, automotive, biomedical, and nano-systems (Smith 2005). A piezoelectric is a type of smart material. The history of piezoelectricity dates to 1880 when Pierre and Jacques Curie discovered the effect in several substances such as the quartz crystal (which is a naturally occurring piezoelectric material). The term piezoelectricity is used for certain materials and substances that generate charge (or voltage) when pressure is applied to them (Cady 1946). These materials are also capable of changing their shape when they are exposed to an electric field. The direct effect is the charge generated due to strain. The converse effect is the mechanical response of the material to the electrical field.

Applications of piezoelectric materials are very broad and they are widely used as actuators and sensors for active vibration control of beams and plates (Hagood and Anderson 1991, Ha *et al* 1992, Ghiringhelli *et al* 1997, Inman and Cudney 2000). The shape and vibration control of aerodynamic surfaces using piezoelectrics started in early 90s. Lazarus *et al* (1991) examined the feasibility of using representative box wing adaptive structures for static aeroelastic control in fixed wing aircraft. Other researchers focused on the application of piezoelectrics to rotor systems to improve their performance and effectiveness. Giurgiutiu *et al* (1994) and Steadman *et al* (1994) showed applications of piezoceramic actuators for vibration and camber control in helicopter blades. Structure-control interaction was employed to develop an adaptive airfoil that can be used in the cyclic and vibration control of the helicopter. For aerodynamic flap actuation, devices range from piezobimorphs (Koratkar and Chopra 2001), piezostacks (Lee and Chopra 2001, Straub *et al* 2001), and piezoelectric/magnetostrictive-induced composite coupled systems (Derham and Hagood 1996, Rogers and Hagood 1997, Bernhard and Chopra 2001, Cesnik and Shin 2001, Kovalovs *et al* 2007).

Although the electrically induced strains are relatively small (around 0.1%) from the piezoelectric material, the force outputs can be relatively large, resulting in high energy density. Response times are also very short which allows for high frequency applications. In addition, piezoelectric materials exhibit high-sensitivity to mechanical deformation which allows them to be used as sensors and energy harvesters. A common synthetic piezoelectric material composition is lead zirconate titanate, PZT for short. A common PZT type, PZT-5A is used in accelerometers, hydrophones, low power structural control, and stable sensors. Another common type, PZT-5H is used in areas requiring sensitive receivers, fine motion control, and low power structural control. The (relatively new) single crystal type piezoelectrics, lead magnesium niobate–lead titanate (PMN–PT) or lead magnesium niobate–lead zirconate titanate (PMN–PZT), are best suited to low induced-stress, high strain, and deflection applications (Wilkie *et al* 2006). The majority of the research in employing piezoelectric materials focuses to the polycrystalline PZT piezoceramic composition due to its moderate electromechanical coupling properties and mechanical practicality. Recent attention is given to single crystal piezoelectrics due to their large electromechanical coupling. The electromechanical and other properties of single crystal piezoelectric materials have been studied in Zhang *et al* (2001), Srinivasan and Spearing (2008), Liu *et al* (2010), Wang *et al* (2011). Sitti *et al* (2001) presented research on using both polycrystalline and single crystal piezoelectric unimorph actuators for micromechanical flapping mechanisms. Park and Kim (2005) presented an analytical development of single crystal Macro-Fiber Composite (MFC) actuators for active twist rotor blades. Wilkie *et al* (2006) incorporated single crystal piezoelectrics into piezocomposite actuators (such as the MFC actuator). The three types of MFC actuators are fabricated and tested with PMN–PT single crystals and PZT-5A and PZT-5H type polycrystalline piezoceramics.

There has been a significant amount of modeling effort of piezoelectric materials as distributed transducers. Analyses range from simple devices such as uniform beams and plates in linear dynamics, to more complicated configurations such as composites under nonlinear and nonuniform loading and dynamics (such as helicopter blades and aircraft wings). Several review papers have been published on the modeling of piezoelectric smart systems (Domeci 1988, Crawley 1994, Chopra 1996, 2000, 2002, Chee *et al* 1998, Sunar and Rao 1999, Giurgiutu 2000, Benjeddou 2000). There are a number of studies in the area of piezoelectric actuation modeling. A majority of the research deals with the modeling of symmetric (bimorph) beams and plates; however the focus of this paper is directed mostly to the asymmetric (unimorph) actuation. The symmetric device theoretically produces only bending strains; in contrast, the asymmetric device has bending–extension coupling. There are two popular sets of assumptions for modeling strain-induced actuation. First, the uniform-strain model assumes that the through-the-thickness variation of strain in the active piezoelectric device is uniform. This assumption holds true for cases where the passive substrate material is relatively thick compared to the active material. The second case allows for the linear variation of strain in the active material and follows the assumptions of the Euler–Bernoulli model. The uniform-strain and Euler–Bernoulli derivations of the strain-induced actuation are presented by Crawley and de Luis (1987) and Crawley and Anderson (1990). These works demonstrated several important results such as the increased effectiveness of the induced-strain actuators for stiffer and thinner bonding layers. Dimitriadis *et al* (1991) presented the behavior of thin plates in response to distributed piezoelectric vibration excitation. Kim and Jones (1991, 1995) presented the optimal design of a bimorph actuator for active acoustic and vibration control. Charette *et al* (1994) demonstrated the actuation and sensing in an asymmetric piezoelectric beam using two separate transducers. Leeks and Weisshaar (1995) showed the optimization of the thickness and distribution of the piezoelectric material in an asymmetric thin plate. Park *et al* (1996) and Park and Chopra (1996) presented models of asymmetric actuators with bending–extension and bending–torsion coupling. Cunningham *et al* (1997) presented an experimental examination of optimum thickness of a unimorph cantilevered beam. Sunar *et al* (2001) presented the robust design of piezoelectric bimorph actuators for structural control using finite element modeling. Lesieutre *et al* (2003) demonstrated the modeling of a dual-unimorph inertial actuator. Li *et al* (2004) presented an analytical derivation of the deflection field for piezoelectric asymmetric actuators. Delas *et al* (2007) demonstrated the optimization of thickness of piezoelectric plate in an asymmetric configuration.

The purpose of the research is to understand the actuation authority of PMN–PZT type piezoelectric materials so that optimal design choices can be employed in lightweight, low power applications. Since single crystal piezoelectric materials are ‘soft’ compared to their polycrystalline counterparts, their optimal design for producing large displacement-to-excitation response differs from the common PZT composition. Their differences in damping characteristics also show a

unique response; therefore this paper presents a parametric experimental and theoretical evaluation to identify (and quantify) the effects of these characteristics. The paper is organized as follows: first, the experimental setup and characteristics of 24 uniform cross-section beams with single crystal and polycrystalline piezoelectrics are presented. These specimens have different substrate materials and different substrate-to-piezoelectric thickness ratios. The important structural and electromechanical properties are presented. Next, the actuation characterization is conducted using an electromechanical model and experimental analysis. Finally, the parameter space is further investigated using the analytical model. The paper concludes with the summary of results.

2. Actuation characteristics

This section presents the actuation performance comparison of the single crystal actuated unimorphs to other unimorphs employing conventional polycrystalline monolithic piezoceramics. The samples are evaluated for their actuation performance via measuring the tip velocity output induced by voltage excitation. The vibration energy harvesting characterization of the samples studied in this paper is presented in Karami *et al* (2011).

2.1. Experimental analysis

A total of 24 unimorphs are fabricated by bonding Ceracomp PMN-PZT (see Ceracomp PMN-PZT), PSI PZT-5A4E (see PSI PZT-5A4E), PSI PZT-5H4E (see PSI PZT-5H4E) type monolithic devices to aluminum and stainless-steel substrates. The substrate materials have four different thicknesses and they all have 5.0 mm width and 30 mm total length. The overhang lengths of the cantilevered beams are set to be 22.5 mm. The length and width dimensions are measured with a digital caliper (with 0.01 mm resolution). Figure 1 shows the cantilevered unimorph beam setup with the laser velocity sensor.

The assumed properties of the piezoelectric devices on the beams are given in table 1. All of the piezoelectric materials used in this section operate in the *31* mode and they are monolithic devices. The single crystal piezoelectrics are manufactured by Ceracomp Co., Ltd., Chungcheongnam-do, South Korea. These crystals are fabricated by the solid-state crystal growth (SSCG) method. The specific model used is CPSC 160-95 type *31* mode PMN–PZT single crystal. These types of single crystals are reported to have (1) high piezoelectric coupling constants (d_{33} and d_{31}), (2) high relative permittivity (K_3^T), (3) low mechanical quality factor (Q_M), (4) low rhombohedral-to-tetragonal transition temperature (T_{RT}) and (5) no internal bias. The other two (polycrystalline) monolithic piezoceramics used are models PZT-5A4E and PZT-5H4E from Piezo Systems, Inc., Woburn, MA, USA. All three piezoelectric devices are poled in the through-the-thickness direction.

The manufacturer, Ceracomp Co. Ltd. provided the typical and the measured properties of the CPSC 160-95 PMN–PZT type single crystals. In table 1, the values presented with

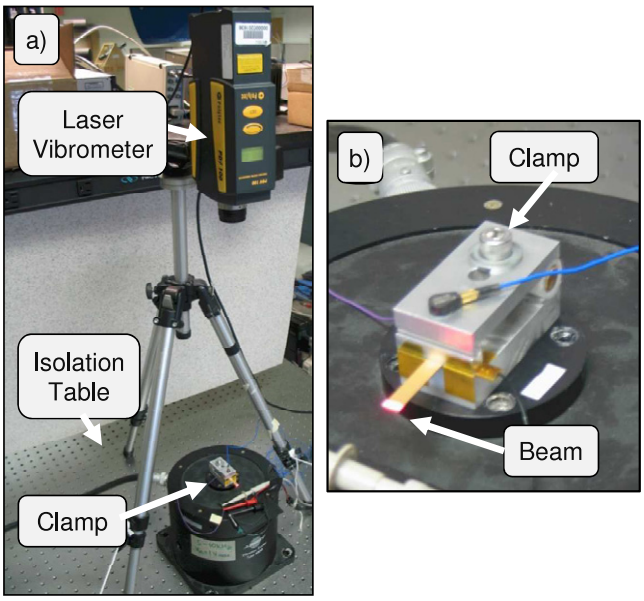

Figure 1. The cantilevered unimorph test setup with a single crystal unimorph installed on the clamp. (a) Complete setup and (b) close-up of the unimorph beam and the clamp.

'*' are average values calculated from the values specific to the piezoelectrics used in this research. Table 2 presents the complete list of the 24 specimens that are tested and their respective thickness properties. Detailed properties of the samples are presented in Bilgen (2010).

Note that the glue thickness has an average measured value of 0.0375 mm and a large standard deviation of 0.0293 mm (for the 24 test specimens). The thicknesses are measured with a digital micrometer (with 0.0001 mm resolution). The substrates are CNC machined to the exact size of the piezoelectric devices and bonded with Tower Hobbies Build-it Thin CA (commonly known as super glue). Samples are bonded by applying pressure by hand; hence a spatial variation in glue thickness for each sample is expected (but not quantified). The electrode surface of the piezoelectrics (that is bonded to the substrate) is accessed by a small hole through the clamped end of the substrate. A small wire is bonded to the 'interior' electrode with a two-part silver epoxy (AI Technology Prime-Solder EG8050) with 0.40 mΩ cm electrical resistivity.

2.2. Analytical model

Piezoelectrics are relatively linear at low electric fields and low mechanical stress levels. In contrast, they show considerable nonlinearity (i.e. hysteresis) at high values of field and stress. Here, the linear actuation regime is investigated. The actuation strain can be modeled like an equivalent thermal strain. The piezoelectric sheet-like actuator can be idealized as an orthotropic material. Following the IEEE Standard (1987), the coupled electromechanical constitutive relations are:

$$D_i = e_{ij}^{\sigma} E_j + d_{im}^{\mathrm{d}} \sigma_m + \alpha_i \Delta T \qquad \text{(Direct)} \qquad (1)$$

$$\varepsilon_k = d_{jk}^{\mathrm{c}} E_j + S_{km}^{\mathrm{E}} \sigma_m + \alpha_k \Delta T \qquad \text{(Converse)} \qquad (2)$$

Table 1. Typical properties of the tested piezoelectric materials.

Piezoelectric properties	Ceracomp PMN-PZT	PSI PZT-5A	PSI PZT-5H
Model	CPSC 160-95	PZT-5A4E	PZT-5H4E
Type	PMN–PZT	II/5A	VI/5H
Thickness, h_p (mm)	0.2800	0.2670	0.2670
Density, ρ_p (kg m^{-3})	8000	7800	7800
Mechanical quality, Q_M	41*	80	32
Relative dielectric constant, K_3^T (1 kHz)	4663*	1900	3800
Electromechanical coupling, k_{33}	0.93	0.72	0.75
Electromechanical coupling, k_{31}	0.88*	0.35	0.44
Strain/applied field, d_{33} (10^{-12} m V^{-1})	2000	390	650
Strain/applied field, d_{31} (10^{-12} m V^{-1})	−1582*	−190	−320
Initial depolarizing field, Ec (10^5 V m^{-1})	n/a	5	3
Coercive field, Ec (10^5 V m^{-1})	4	12	8
Maximum voltage (V)	n/a	±134	±80
Curie temperature, T_C (°C)	160	350	230
Compliance, s_{11}^E (10^{-12} m^2 N^{-1})	77.7*	16.4	16.5

Table 2. Thickness properties of unimorph beams with PZT-5A, PZT-5H and PMN–PZT type polycrystalline and single crystal piezoelectrics. (Substrate thickness (h_s); glue thickness (h_g); aluminum (Al); stainless-steel (Ss).)

Sample	Type	Subs.	h_s (mm)	h_g (mm)
5H01	PZT-5H	Al	0.3861	0.0287
5H02	PZT-5H	Ss	0.3861	0.0559
SC05	PMN–PZT	Ss	0.1095	0.0197
SC06	PMN–PZT	Ss	0.2581	0.0182
SC07	PMN–PZT	Ss	0.3858	0.0075
SC08	PMN–PZT	Ss	0.5108	0.0073
SC09	PMN–PZT	Ss	0.6299	0.0162
SC10	PMN–PZT	Al	0.1400	0.0759
SC11	PMN–PZT	Al	0.2540	0.0637
SC12	PMN–PZT	Al	0.3866	0.1259
SC13	PMN–PZT	Al	0.5060	0.0659
SC14	PMN–PZT	Al	0.8189	0.0583
SC16	PMN–PZT	Al	0.1328	0.0870
SC17	PMN–PZT	Ss	0.3868	0.0027
5H20	PZT-5H	Ss	0.1092	0.0231
5H21	PZT-5H	Ss	0.2573	0.0216
5H22	PZT-5H	Ss	0.3861	0.0368
5H23	PZT-5H	Ss	0.5088	0.0323
5H24	PZT-5H	Ss	0.6266	0.0208
5A25	PZT-5A	Ss	0.1069	0.0198
5A26	PZT-5A	Ss	0.2598	0.0284
5A27	PZT-5A	Ss	0.3805	0.0361
5A28	PZT-5A	Ss	0.5067	0.0246
5A29	PZT-5A	Ss	0.6215	0.0234

where D_i is the electric displacement, ε_k is the strain, E_j is the applied electric field and σ_m is stress. d_{im}^d and d_{jk}^c are the direct and converse piezoelectric coefficients respectively. The dielectric permittivity is denoted by e_{ij}^σ (measured at constant stress state) and the elastic compliance matrix is denoted by S_{km}^E (measured at constant electric field). The thermal expansion coefficients, α_i and α_k, and the temperature change, ΔT are left in the constitutive relationships for completeness.

The linear electromechanical dynamic actuation model of a cantilevered unimorph beam is briefly described in this section. As noted earlier, the uniform-strain and Euler–Bernoulli derivations of the strain-induced actuation are presented by Crawley and de Luis (1987) and Crawley and Anderson (1990), the asymmetric actuator equations are presented by Park *et al* (1996), and the modal treatment of forced vibrations of a cantilevered beam is presented in Inman (2007). The unimorph (asymmetric) piezoelectric actuators considered in this paper operate in the *31* mode of piezoelectricity. For the case of *31* mode actuation, the strain in the longitudinal direction is:

$$\varepsilon_1 = d_{31}E_3 + S_{11}\sigma_1 + S_{12}\sigma_2 + S_{13}\sigma_3 \tag{3}$$

where ε_1 is the strain (in the direction of beam axis), d_{31} is the piezoelectric constant, E_3 is the electric field (in the through-the-thickness direction), S is the elastic compliance, and σ is the stress.

Since the beam cross-section is small with respect to the bending wavelength at the highest frequency of interest, the unimorph cantilever is modeled as a uniform Euler–Bernoulli beam. The free vibrations of the beam are governed by Banks and Inman (1991):

$$\frac{\partial^2 M(x,t)}{\partial x^2} + c_s I\frac{\partial^5 w(x,t)}{\partial x^4 \partial t} + c_a\frac{\partial w(x,t)}{\partial t} + \rho A\frac{\partial^2 w(x,t)}{\partial t^2} = 0 \tag{4}$$

where $M(x,t)$ is the internal bending moment, $c_s I$ is the Kelvin–Voigt damping term, $w(x,t)$ is the transverse deflection, c_a is the viscous damping coefficient and ρA is the mass per unit length of the beam. The voltage induced electric field, E_3, can be written in terms of the applied voltage, $v(t)$ and the distance between the electrodes, h_p (which is equivalent to the thickness of the piezoelectric sheet). By replacing the moment term in equation (4) with the summation of internal moment term and piezoelectric induced moment (Cremer *et al* 1973), the equation for the forced flexural vibrations of the beam (Gibbs and Fuller 1992) including Kelvin–Voigt and viscous damping (Banks and Inman 1991) becomes:

$$YI\frac{\partial^4 w(x,t)}{\partial x^4} + c_s I\frac{\partial^5 w(x,t)}{\partial x^4 \partial t} + c_a\frac{\partial w(x,t)}{\partial t} + \rho A\frac{\partial^2 w(x,t)}{\partial t^2} = -\alpha\left(\frac{\mathrm{d}\delta(x)}{\mathrm{d}x} - \frac{\mathrm{d}\delta(x-L)}{\mathrm{d}x}\right) \tag{5}$$

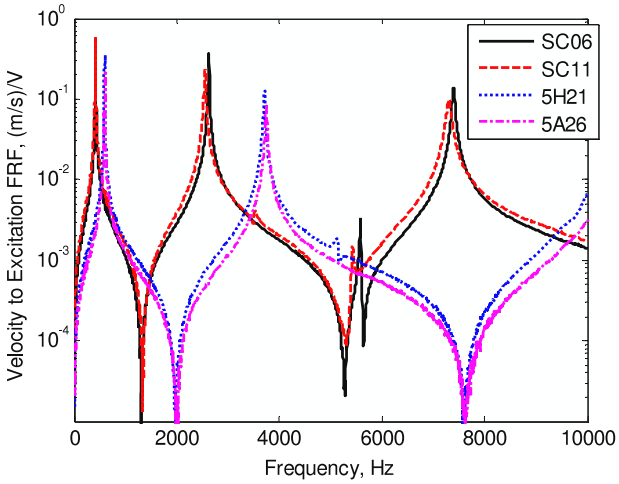

Figure 2. Experimental tip velocity to harmonic voltage excitation FRF of four (out of 24) clamped-free unimorphs.

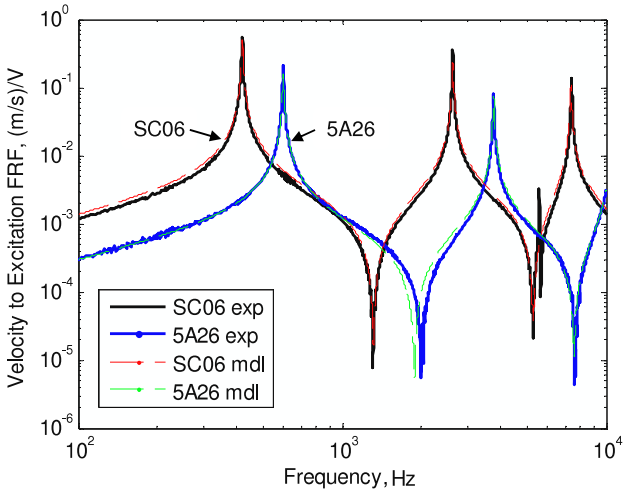

Figure 3. Comparison of experimental (exp) tip velocity to harmonic voltage excitation FRF to model (mdl) prediction.

where YI is the bending stiffness of the unimorph, α is the forcing term, δ is the delta function and L is the overhang length. Following Crawley and de Luis (1987), the forcing term is given by:

$$\alpha = \Lambda Y_{\mathrm{p}} b_{\mathrm{p}} (h_{\mathrm{pt}}^2 - h_{\mathrm{pb}}^2)/2 \tag{6}$$

where $\Lambda = v(t)d_{31}/h_{\mathrm{p}}$ is the piezoelectric strain, Y_{p} is the modulus of the piezoelectric, b_{p} is the width of the substrate (and the piezoelectric). The distances of the piezoelectric surfaces (in the thickness direction) from the neutral axis are denoted by h_{pt} for the top surface and h_{pb} for the bottom surface. Assuming that the voltage excitation is harmonic, (where $v(t) = V_0 \mathrm{e}^{\mathrm{j}\omega t}$, V_0 is the voltage amplitude and ω is the driving frequency),the physical steady state response of the beam represented by equation (5) is obtained as:

$$w(x,t) = \int_{m=1}^{\infty} \frac{-\chi_m \phi_m(x)}{\omega_m^2 - \omega^2 + 2\zeta_m \omega_m \mathrm{j}\omega} V_0 \mathrm{e}^{\mathrm{j}\omega t} \tag{7}$$

where χ_m is the modal coupling term, ϕ_m is the mass normalized eigenfunction, ω_m is the undamped natural frequency, ζ_m is the modal mechanical damping ratio of the mth mode. Equation (7) follows from computing the forced response of a distributed parameter system (see Inman 2007).

2.3. Evaluation of results

The tip velocity to harmonic voltage excitation frequency response function (FRF) is measured through experimentation for all 24 unimorph beams. A Polytec PDV-100 laser vibrometer and a Siglab 20-42 frequency analyzer is used to measure the tip velocity of the cantilevers. A virtual sine sweep is used for the FRF measurements, where the excitation is a pure sine tone at constant frequency. The frequency is incremented only when the transients have decayed from the previous frequency. This method is utilized to avoid windowing and transients caused by more common (and faster) techniques, such as a chirp excitation. The 500 mV peak pure sine tone excitation signal (from the Siglab Analyzer) is buffered through an HP 6826A bipolar amplifier with a fixed unity gain. The acquisition is conducted in the 5 Hz–10 kHz frequency range, with 1 Hz resolution. Three complete cycles are recorded at each frequency and averaged. The laser measurement is taken at 21.4 mm from the base of the clamped-free beams. As noted earlier, the overhang lengths of the beams are 22.5 mm. Figure 2 presents tip velocity per excitation voltage FRF of the four unimorph beams with approximately 0.25 mm thick substrates. Samples SC06, 5H21 and 5A26 have stainless-steel substrates, and sample SC11 has an aluminum substrate. The first three bending resonances can be seen for the two single crystal specimens.

The solution given in equation (7) is used to predict the frequency response function of the cantilevered unimorphs. A damping ratio of 0.005 is assumed for all modes. The Young's moduli for aluminum and steel substrates are assumed to be 70 GPa and 200 GPa respectively. The mass densities of the aluminum and steel are assumed to be 2700 kg m^{-3} and 7800 kg m^{-3} respectively. The shear strength for the glue layer is approximately 31 MPa. As noted earlier, the glue thickness has a large variation and this variation is an important source of error between the model and experiments. Figure 3 presents the comparison of model and the experiments (labeled as mdl and exp respectively) for two unimorph samples, SC06 and 5A26.

The model is in very good agreement with the experiments for the first three operational modes in the complete acquisition bandwidth. It is important to note that the bending stiffness used to generate these plots is adjusted so that the model prediction of the first bending resonance matches the experimental case. This is done to show that the specimens demonstrate the desired separation between each resonance, and that the assumed clamped-free beam mode shapes are valid. In reality, there is a small mismatch (less than 5%) between the experimental and the model prediction for the first resonance frequency. The prediction for second and third bending resonances shows a shift in the same direction relative to the shift observed in the first frequency. It is also important

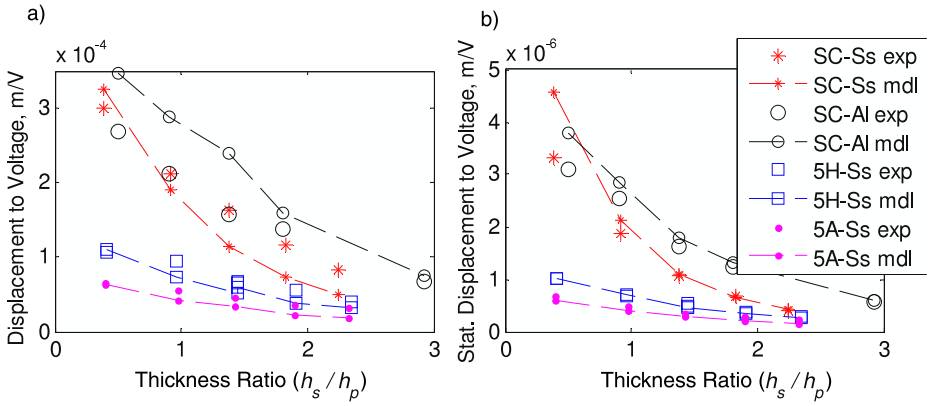

Figure 4. Comparison of experimental (exp) and theoretical (mdl) peak tip displacement response to harmonic voltage excitation for all 24 specimens. (a) Peak displacement at first bending resonance frequency. (b) Quasi-static displacement.

to note that amplitude adjustments (i.e. correction factor to the coupling or adjustment of the damping ratio) are not applied, showing that the forcing term (equation (6)) is successful in predicting the piezoelectric induced moment in the beam.

In figure 4, the peak tip displacement response to harmonic voltage excitation is presented against the substrate-to-piezoelectric thickness ratio. The tip displacement FRFs are calculated from the tip velocity to harmonic voltage excitation FRF measurements. The thicknesses of piezoelectrics and the substrates are presented in tables 1 and 2 respectively. As noted earlier, the theoretical bending stiffness is matched to the experimental case using the first bending resonance frequency. The peak displacement-to-voltage excitation response (to harmonic excitation) at the first bending resonance frequency is presented in figure 4(a). The quasi-static displacement-to-voltage excitation response (calculated at 5 Hz) is given in figure 4(b). Although experimentally not achieved, it is important to note that (1) an optimum thickness ratio would be observed in figure 4 if more samples with thinner substrates were available and (2) the out-of-plane displacement would be zero for zero substrate thickness (hence for zero thickness ratio). The theoretical predictions (in figure 4) are presented only for the respective experimental cases, therefore the theoretical optimum thickness ratios are also not shown. The theoretical response (and the optimum thickness ratio) for a PMN–PZT single crystal driven unimorph (with ideal geometric and geometric properties) will be presented in section 2.4.

In figure 4, the y-axis scale is linear; therefore it is easier to see the amplitude prediction error for different substrate materials and thickness ratios. Figure 3 shows good dynamic spectrum prediction; in contrast, figure 4 shows the amplitude error due to several reasons, one being the assumed damping ratio (of 0.005) for all modes and all specimens. From the resonance response (figure 4(a)), the effective damping assumption appears to under predict response for steel substrates and over predict response for aluminum substrates. This conclusion is valid for high thickness ratios in which the dominant dissipation mechanism is assumed to be the substrate material. In addition to damping, it is also known that the Euler–Bernoulli assumptions and the perfect bonding

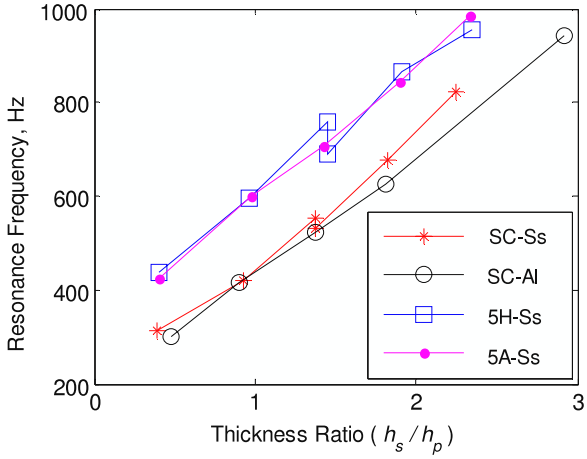

Figure 5. First bending resonance frequency (at the peak displacement operation point) of all 24 specimens. Response is to harmonic voltage excitation.

layer assumption lose validity as the thickness ratio approaches low values (Chopra 2002). This is better seen in the quasi-static response shown in figure 4(b) where the effect of the assumed damping ratio on the model prediction is diminished. Figure 4(b) clearly shows the over prediction of the response (for low thickness ratios) because of the perfect bonding assumption. Figure 5 presents the first bending resonance of the specimens in response to harmonic excitation.

Both for dynamic and quasi-static response, the single crystal PMN–PZT type unimorphs show superior actuation response when compared to polycrystalline PZT-5A and PZT-5H type ceramics. It is both experimentally and theoretically observed (from figure 4) that the unimorph devices driven with PMN–PZT single crystal materials produce approximately 2.8–2.1 times the peak displacement when compared to the PZT-5H for the thickness ratio range of 0.4–2.3 respectively (for same applied voltage and substrate material and geometry). Likewise, the PMN–PZT unimorph produces approximately 4.6–2.8 times the peak displacement when compared to the PZT-5A material, also for the thickness ratio range of 0.4–2.3 respectively. However, due to their low

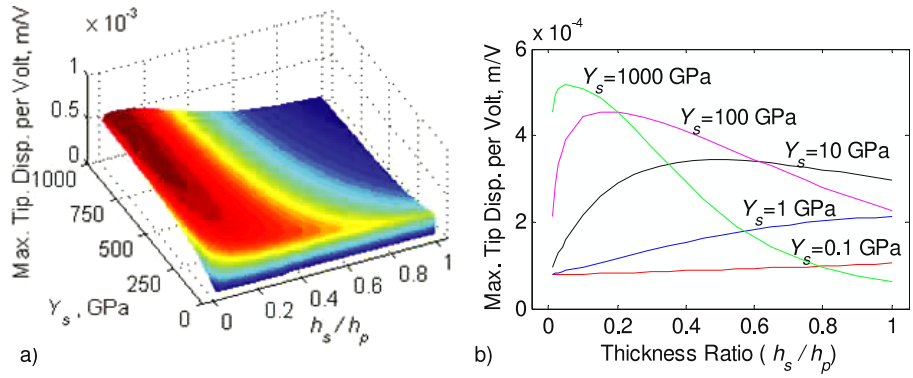

Figure 6. Theoretical peak displacement response of single crystal PMN–PZT driven unimorph beam to harmonic voltage excitation for a range of substrate Young's moduli and thickness ratios. (a) 3D and (b) 2D representations.

stiffness, the single crystal PMN–PZT type piezoelectrics are not as effective as it appears from their large piezoelectric coupling values. It is also noted that the thickness ratios of the tested specimens are larger than the predicted optimum thickness ratio (that results in highest mechanical output). Also note that the active material stiffness with respect to the substrate stiffness plays an important role in addition to the substrate-to-piezoelectric thickness ratio. Single crystal piezoelectrics are significantly softer when compared to polycrystalline ceramics as presented in table 1.

2.4. Parametric analysis

This section presents the theoretical actuation response (and the optimum thickness ratio) for a PMN–PZT single crystal driven unimorph (with ideal material and geometric properties). The parametric study is conducted using the solution given in equation (7). The mechanical output (quantified in terms of peak tip displacement response to harmonic voltage excitation) is calculated for a range of 'ideal' substrate Young's moduli and substrate-to-piezoelectric thickness ratios. Figure 6 presents the mechanical response of the ideal unimorph beam with a single crystal PMN–PZT piezoelectric material (with the properties given in table 1) and a substrate material with a constant density of 2700 kg m^{-3}. In the figure, the substrate Young's modulus is varied between 0.01 GPa through 1000 GPa, representing materials from rubbers to carbon nanotubes. Similar to the tested specimens, the beam has 5.0 mm width and 22.5 mm overhang length. As noted earlier, the out-of-plane displacement output is zero for a zero substrate thickness (hence zero thickness ratio). In figure 6, low thickness ratios (<0.05) are not plotted in order to aid the clarity data of interest. Both two-dimensional and three-dimensional plots are used to aid the discussion from a qualitative and a quantitative point of view.

There are several important observations that can be deduced from figure 6: (1) there is an optimum thickness ratio that occurs for any choice of substrate Young's modulus and the out-of-plane displacement approaches zero as the substrate thickness is reduced to zero. This result is consistent with the observations made by Park and Chopra (1996), Inman and Cudney (2000) and Chopra (2002) for the static actuation. (2) Increasing the substrate Young's modulus (while keeping it sufficiently thin so that only in-plane stiffness is increased) increases the out-of-plane displacement only up to a certain point. Beyond this 'saturation' level, the substrate appears (axially) infinitely stiff to the piezoelectric material. It is important to note that the large bending strains and stresses are assumed to be acceptable for the substrate material and the piezoelectric material (i.e. the material is still in the linear elastic region). In addition, at low thickness ratios, the shear stress at the glue layer is very large; therefore the assumption of perfect bonding layer may no longer be valid. Note that the maximum tip displacement of the unimorph occurs at different resonance frequencies for different substrate materials and thicknesses. The effect of the substrate material Young's modulus shows as change in the maximum displacement at the predicted optimum thickness ratio.

3. Conclusions

A total of 24 small unimorph specimens with PMN–PZT, PZT-5H and PZT-5A type piezoelectrics are evaluated for their tip velocity and displacement output response to harmonic voltage excitation. Single crystal type unimorphs demonstrated superior actuation response when compared to unimorphs with polycrystalline ceramics. The unimorph devices driven with PMN–PZT single crystal materials produce approximately 2.8–2.1 times the peak displacement when compared to the PZT-5H for the thickness ratio range of 0.4–2.3 respectively (for same applied voltage and substrate material and geometry). Likewise, the PMN–PZT unimorph produces approximately 4.6–2.8 times the peak displacement when compared to the PZT-5A material, also for the thickness ratio range of 0.4–2.3 respectively. The PMN–PZT type single crystals used here are reported to have (1) high piezoelectric coupling constant (d_{33} and d_{31}), (2) high relative permittivity (K_3^T), (3) low mechanical quality factor (Q_M), (4) low rhombohedral-to-tetragonal transition temperature (T_{RT}) and (5) no internal bias. The single crystals are known to be 'soft' piezoelectrics which is a major practical issue. During the fabrication and testing of the single crystal based unimorphs, several specimens were broken with very small forces applied. The lack of grain boundaries (as in the

polycrystalline material) makes the single crystals very 'brittle' and susceptible to stress concentrations. Another important limitation is the low transition temperature. The electrodes cannot be soldered using conventional solder materials and temperatures, therefore relatively expensive and slow methods (such as two-part conductive epoxies) have to be used for wiring.

Acknowledgments

The authors are grateful for the support of Air Force Office of Scientific Research (AFOSR) Grant Number FA9550-09-1-0625 'Simultaneous Vibration Suppression and Energy Harvesting' under the direction of 'Les' Lee. The authors also gratefully acknowledge the partial financial support from the Office of Naval Research through MURI grant No. N00014-08-1-0654. Additional support of the US Department of Commerce, National Institute of Standards and Technology, Technology Innovation Program, Cooperative Agreement Number 70NANB9H9007 is also acknowledged. The authors acknowledge funding from the European Research Council through grant number 247045 entitled 'Optimisation of Multiscale Structures with Applications to Morphing Aircraft'. The authors would like to thank colleagues at the Center for Intelligent Material Systems and Structures (CIMSS) for their support with experiments and theoretical questions.

References

Banks H T and Inman D J 1991 On damping mechanisms in beams *ASME J. Appl. Mech.* **58** 716–23

Benjeddou A 2000 Advances in piezoelectric finite element modeling of adaptive structural elements: a survey *Comput. Struct.* **76** 347–63

Bernhard A P F and Chopra I 2001 Analysis of a Bending-Torsion coupled actuator for a smart rotor with active blade tips *Smart Mater. Struct.* **10** 35–52

Bilgen O 2010 Aerodynamic and electromechanical design modeling and implementation of piezocomposite airfoils *PhD Dissertation* Mechanical Engineering Department, Virginia Tech, Blacksburg, Virginia http://scholar.lib.vt.edu/theses/available/etd-08142010-142319/

Cady W G 1946 *Piezoelectricity: An Introduction to the Theory and Applications of Electromechanical Phenomena in Crystals* (New York: McGraw Hill)

Ceracomp PMN-PZT (Online data sheet) http://www.ceracomp.com/sub/sub03_01_05.php

Cesnik C E S and Shin S J 2001 On the twist performance of a multiple-cell active helicopter blade *Smart Mater. Struct.* **10** 53–61

Charette F, Guigou C, Berry A and Plantier G 1994 Asymmetric actuation and sensing of a beam using piezoelectric materials *J. Acoust. Soc. Am.* **96** 2272–83

Chee C Y K, Tong L and Steven G P 1998 A review on the modeling of piezoelectric sensors and actuators incorporated in intelligent structures *J. Intell. Mater. Syst. Struct.* **9** 3–19

Chopra I 1996 Review of current status of smart structures and integrated systems *Proc. SPIE* **2717** 20–62

Chopra I 2000 Status of application of smart structures technology to rotorcraft systems *J. Am. Helicopter Soc.* **45** 228–52

Chopra I 2002 Review of state of art of smart structures and integrated systems *AIAA J.* **40** 2145–87

Crawley E F 1994 Intelligent structures for aerospace: a technology overview and assessment *AIAA J.* **32** 1689–99

Crawley E F and Anderson E H 1990 Detailed models of piezoceramic actuation of beams *J. Intell. Mater. Syst. Struct.* **1** 4–25

Crawley E F and de Luis J 1987 Use of piezoelectric actuators as elements of intelligent structures *AIAA J.* **25** 1373–85

Cremer L, Heckel M and Ungar C A 1973 *Structure-Borne Sound* (Berlin: Springer)

Cunningham M J, Jenkins D F L and Bakush M M 1997 Experimental investigation of optimum thickness of a piezoelectric element for cantilever actuation *Science, Measurement & Technology IEE Proc.* A **144** 45–48

Delas O, Berry A, Masson P and Pasco Y 2007 Optimizing the thickness of piezoceramic actuators for bending vibration of planar structures *J. Intell. Mater. Syst. Struct.* **18** 1191–201

Derham R C and Hagood N W 1996 Rotor design using smart materials to actively twist blades *Proc. American Helicopter Society 52nd Annual Forum* vol 2 pp 1242–52

Dimitriadis E K, Fuller C R and Rogers C A 1991 Piezoelectric actuators for distributed vibration excitation of thin plates *J. Vib. Acoust.* **113** 100–7

Domeci M C 1988 Recent progress in the dynamic applications of piezoelectric crystals *Shock Vib. Dig.* **20** 3–20

Ghiringhelli G L, Masarati P and Mantegazza P 1997 Characterization of anisotropic, non-homogeneous beam sections with embedded piezo-electric materials *J. Intell. Mater. Syst. Struct.* **8** 842–58

Gibbs G P and Fuller C R 1992 Excitation of thin beams using asymmetric piezoelectric actuators *J. Acoust. Soc. Am.* **92** 3221–7

Giurgiutiu V, Chaudhry Z and Rogers C A 1994 Engineering feasibility of induced-strain actuators for rotor blade active vibration control *Proc. SPIE* **2190** 107–122

Giurgiutu V 2000 Review of smart-materials actuation solutions for aeroelastic and vibration control *J. Intell. Mater. Syst. Struct.* **11** 525–44

Ha S K, Keilers C and Chang F K 1992 Finite element analysis of composite structures containing distributed piezoceramic sensors and actuators *AIAA J.* **30** 772–80

Hagood N W and Anderson E H 1991 Simultaneous sensing and actuation using piezoelectric materials *Proc. SPIE* **1543** 409–21

IEEE Standard 1987 Institute of Electrical and Electronics Engineers Standard on Piezoelectricity *Standard 176 ANSI/IEEE*

Inman D J and Cudney H H 2000 *Structural and Machine Design Using Piezoceramic Materials: A Guide for Structural Design Engineers Final Report to NASA Langley Research Center* (NASA Langley Grant NAG-1-1998, April 30 2000)

Inman D J 2007 *Engineering Vibration* (New Jersey: Prentice Hall)

Karami M A, Bilgen O, Inman D J and Friswell M I 2011 Experimental and analytical parametric study of single crystal unimorph beams for vibration energy harvesting *IEEE Trans. Ultrason. Ferroelectr. Freq. Control* at press

Kim S J and Jones J D 1991 Optimal-design of piezoactuators for active noise and vibration control *AIAA J.* **29** 2047–53

Kim S J and Jones J D 1995 Influence of piezo-actuator thickness on the active vibration control of a cantilever beam *J. Intell. Mater. Syst. Struct.* **6** 610–23

Koratkar N A and Chopra I 2001 Wind tunnel testing of a mach-scaled rotor model with trailing-edge flaps *Smart Mater. Struct.* **10** 1–14

Kovalovs A, Barkanov E and Gluhihs S 2007 Active twist of model rotor blades with D-spar design *Transport* **22** 38–44 ISSN 1648-4142

Lazarus K B, Crawley E F and Bohlmann J D 1991 Static aeroelastic control using strain actuated adaptive structures *J. Intell. Mater. Syst. Struct.* **2** 386–410

Lee T and Chopra I 2001 Design of piezostack-driven trailing-edge flap actuator for helicopter rotors *Smart Mater. Struct.* **10** 15–24

Leeks T J and Weisshaar T A 1995 Optimization of unsymmetric actuators for maximum panel deflection control *Proc. SPIE* **2443** 62–74

Lesieutre G A, Rusovici R, Koopman G H and Dosch J J 2003 Modelling and characterization of a piezoceramic inertial actuator *J. Sound Vib.* **261** 93–107

Li Q, Lovell M, Mei J and Clark W 2004 A study of displacement distribution in a piezoelectric heterogeneous bimorph *J. Mech. Des.* **126** 757–62

Liu D, Zhang Y, Wang W, Ren B, Zhang Q, Jiao J, Zhao X and Luo H 2010 Complete set of elastic dielectric and piezoelectric coefficients of [−101] poled $0.23Pb(In_{1/2}Nb_{1/2}O_3)$–$0.45Pb(Mg_{1/3}Nb_{2/3})O_3$–$0.32PbTiO_3$ single crystals *J. Alloys Compounds* **506** 428–33

Park C and Chopra I 1996 Modeling piezoceramic actuation of beams in torsion *AIAA J.* **34** 2582–9

Park C, Walz C and Chopra I 1996 Bending and torsion models of beams with induced-strain actuators *Smart Mater. Struct.* **5** 98–113

Park J S and Kim J H 2005 Analytical development of single crystal macro fiber composite actuators for active twist rotor blades *J. Smart Mater. Struct.* **14** 745–53

PSI PZT-5A4E (Online data sheet for industry type 5A (Navy Type II) piezoceramic) http://www.piezo.com/prodsheet3disk5A.html

PSI PZT-5H4E (Online data sheet for industry type 5H (Navy Type VI) piezoceramic) http://www.piezo.com/prodsheet2sq5H.html

Rogers J P and Hagood N W 1997 Design and manufacture of an integral twist-actuated rotor blade *38th AIAA/ASME/ASCE/AHS/ASC Structures Structural Dynamics and Materials Conf. and Adaptive Structures Forum (Reston, VA)*

Sitti M, Campolo D, Yan J and Fearing R S 2001 Development of PZT and PZN–PT based unimorph actuators for micromechanical flapping mechanisms *IEEE Int. Conf. on Robotics and Automation (Seoul, Korea)*

Smith R C 2005 *Smart Material Systems: Model Development* (Philadelphia, PA: SIAM)

Srinivasan P and Spearing S M 2008 Optimal materials selection for bimaterial piezoelectric microactuators *J. Microelectromech. Syst.* **17** 462–72

Steadman D L, Griffin S L and Hanagud S V 1994 Structure-control interaction and the design of piezoceramic actuated adaptive airfoils *AIAA/ASME Adaptive Structures Forum (Hilton Head, SC)* AIAA-1994-1747

Straub F K, Ngo H T, Anand V and Domzalski D B 2001 Development of a piezoelectric actuator for trailing-edge flap control for full scale rotor system *Smart Mater. Struct.* **10** 25–34

Sunar M and Rao S S 1999 Recent advances in sensing and control of flexible structures via piezoelectric materials technology *Appl. Mech. Rev.* **52** 1–16

Sunar M, Hyder S J and Yilbas B S 2001 Robust design of piezoelectric actuators for structural control *Comput. Meth. Appl. Mech. Eng.* **190** 6257–70

Wang F, Shi W, Or S W, Zhao X and Luo H 2011 Cryogenic transverse and shear mode properties of $(1-x)Pb(Mg_{1/3}Nb_{2/3})O_3$–$xPbTiO_3$ single crystal with the optimal crystallographic direction *Mater. Chem. Phys.* **125** 718–22

Wilkie W K, Inman D J, Lloyd J M and High J W 2006 Anisotropic laminar piezocomposite actuator incorporating machined PMN–PT single-crystal fibers *J. Intell. Mater. Syst. Struct.* **17** 15–28

Zhang R, Jiang B and Cao W 2001 Elastic piezoelectric and dielectric properties of multidomain $0.67Pb(Mg_{1/3}Nb_{2/3})O_3$–$0.33PbTiO_3$ single crystals *J. Appl. Phys.* **90** 3471–5